Dalton Transactions

Accepted Manuscript

ROYAL SOCIETY OF CHEMISTRY

www.rsc.org/dalton

Precisely tunable magnetic phase transition temperature, T_C, through formation of molecule alloy in $[Ni_xPt_{1-x}(mnt)_2]^-$-based spin systems (mnt^{2-} = maleonitriledithiolate, x = 0.09-0.91)

Guo-Jun Yuan,[a] Hao Yang,[a] Shao-Xian Liu, [a] Jian-Lan Liu [a] and Xiao-Ming Ren *[a,b]

[a] State Key Laboratory of Materials-Oriented Chemical Engineering and College of Science, Nanjing University of Technology, Nanjing 210009

[b] College of Materials Science and Engineering, Nanjing University of Technology, Nanjing 210009

Tel.: +86 25 58139476

Fax: +86 25 58139481

Email: xmren@njtech.edu.cn

Abstract: Nine molecular substitutional alloys with a formula $[Cl\text{-}BzPy][Ni_xPt_{1-x}(mnt)_2]$ (x = 0.09-0.91) were prepared by mixing the isostructural $[Cl\text{-}BzPy][Ni(mnt)_2]$ and $[Cl\text{-}BzPy][Pt(mnt)_2]$ in acetonitrile according to the molar ratio of x/(1-x), where mnt^{2-} = maleonitriledithiolate, $Cl\text{-}BzPy^{+}$ = 1-(4'-chloro-benzyl)pyridinium. Each alloy compound is isostructural with the parent compounds and shows a magnetic transition; the T_C decreases linearly with the molar fraction x, indicating that T_C is precisely tunable in this alloy system.

Keywords: Metal-bis-dithiolene salt, molecular substitutional alloy, spin-Peierls transition, tunable critical temperature

Introduction

The spin-Peierls (SP) transition occurs in an antiferromagnetically (AFM) coupled S = 1/2 Heisenberg or XY chain where the magnetoelastic coupling induces a progressive lattice dimerization. As a result, a gap opens in the magnetic excitation spectrum to separate the diamagnetic ground state from a continuum of excited states.[1–3] The spin-Peierls or spin-Peierls-like transition phenomenon has been found in both inorganic and organic compounds.[2, 4–8] The true one-dimensionality of the lattices is not obtained in inorganic compound and the transition temperature is lower owing to the strong inter-chain interaction. Contrarily, the presence of large counterions or other non-covalent interaction in organic system leads to relatively weak inter-chain interaction, providing softness to the lattice and allowing the spin dimerization to occur at much higher temperature.[9] In addition to the transition temperature T_C, the difference of inter-chain interaction between inorganic and organic compounds also result in the distinction that the impurity doping influences on the features of both transition and magnetic ground state.[10-13]

In previous studies, we achieved two isostructural spin-Peierls-like compounds, [Cl-BzPy][Ni(mnt)$_2$] and [Cl-BzPy][Pt(mnt)$_2$] (Cl-BzPy$^+$ = 4'-chlorobenzyl-1-pyridinium and mnt^{2-} = maleonitriledithiolate).[14,15] Given that there is larger HOMO overlap between neighboring anions within a [Pt(mnt)$_2$]$^-$ than a [Ni(mnt)$_2$]$^-$ stack, AFM coupling interaction is stronger in [ClBzPy][Pt(mnt)$_2$] than [ClBzPy][Ni(mnt)$_2$], which leads to [ClBzPy][Pt(mnt)$_2$] ($T_C \approx 275$ K) shows higher T_C by comparison of [ClBzPy][Ni(mnt)$_2$] ($T_C \approx 106$ K) (This can be understood since $k_BT_C = 2.28pJexp(-1/\lambda)$ in a spin-Peierls system, where J is the magnetic coupling constant in a regular spin chain and p is the only weakly temperature dependent constant),[2] even if two compounds show quite similar cell parameters, packing structure and magnetic feature. In this paper, the molecular alloys [Cl-BzPy][Ni$_x$Pt$_{1-x}$(mnt)$_2$] (x = 0.09-0.91; ref. Scheme 1) were prepared using the isomorphic substitution approach owing to [Ni(mnt)$_2$]$^-$ and [Pt(mnt)$_2$]$^-$ anions possessing the same charge and extremely analogous molecular geometry, and found

that the magnetic transition temperature, T_C, is precisely tunable in this molecular alloy family through alternation of the molar proportions of $[Ni(mnt)_2]^-$ to $[Pt(mnt)_2]^-$ component.

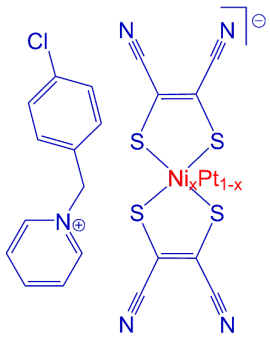

Scheme 1 Illustration for molecule structure of [Cl-BzPy][Ni_xPt_{1-x}(mnt)$_2$] (x = 0.09-0.91).

Experimental section

Preparation of compounds

Chemicals and materials. All reagents and chemicals were purchased from commercial sources and used without further purification. Compounds [Cl-BzPy][Ni(mnt)$_2$] and [Cl-BzPy][Pt(mnt)$_2$] were prepared following the published procduces.[14,15]

[Cl-BzPy][Ni_xPt_{1-x}(mnt)$_2$] (x = 0.09-0.91). [Cl-BzPy][Ni(mnt)$_2$] and [Cl-BzPy]-[Pt(mnt)$_2$] were mixed in acetonitrile with a molar ratio of [Cl-BzPy][Ni(mnt)$_2$] /[Cl-BzPy][Pt(mnt)$_2$] = x/(1-x). The mixed solution was evaporated at ambient temperature to give crystals of **[Cl-BzPy][Ni_xPt_{1-x}(mnt)$_2$]** (x = 0.09-0.91), which are suitable for X-ray single structure analyses and other measurements.

Physical measurements

Elemental analyses (C, H and N) were performed with an Elementar Vario EL III analytical instrument. The Ni and Pt contents in each alloy compound was determined by inductively coupled plasma-mass spectra (ICP-MS, Optima 5300DV, USA) and energy dispersive spectrometer and EDS mapping of Ni and Pt elements (EDS, S-3400N Π, Japan). Infrared (IR) spectra were recorded on a Bruker

VERTEX80V Fourier transform infrared spectrometer (KBr disc) under vacuum. Power X-ray diffraction (PXRD) data were collected on a Bruker D8 Advance powder diffractometer operating at 40 kV and 40 mA for Cu Kα radiation with λ = 1.5418 Å. Magnetic susceptibility data were measured for polycrystalline samples over temperature range of 2-300 K using a Quantum Design MPMS-5S superconducting quantum interference device (SQUID) magnetometer. Differential scanning calorimetry (DSC) were carried out on a Q2000 V24.9 Build 121 instrumental in the temperature range between -180 and 20 °C (93-293 K).

X-ray single crystal structural analyses

X-ray single crystal diffraction data were collected at 296 K with graphite monochromated Mo Kα (λ = 0.71073 Å) on a CCD area detector (Bruker-SMART). Data reductions and absorption corrections were respectively performed with the SAINT and SADABS software packages.[16] Structures were solved by direct method using the SHELXL-97 software package.[17] The occupied factors of Ni and Pt were refined in each [Cl-BzPy][$Ni_xPt_{1-x}(mnt)_2$] compound. The non-hydrogen atoms were anisotropically refined using the full-matrix least-squares method on F^2. All hydrogen atoms were placed at the calculated positions and refined riding on the parent atoms. The details about data collection, structure refinement and crystallography are summarized in Table 1.

Results and discussion

Alloy sample characterization and spectroscopic analysis

The molar ratio of [Cl-BzPy][$Ni(mnt)_2$] to [Cl-BzPy][$Pt(mnt)_2$] in the starting materials, the elemental analyses for C, H and N as well as the occupation factor of Ni/Pt ion in the [Cl-BzPy][$Ni_xPt_{1-x}(mnt)_2$] (x = 0.09-0.91) crystal structure are presented in Table 2, indicating that the molar ratio between Ni and Pt in the **[Cl-BzPy][$Ni_xPt_{1-x}(mnt)_2$]** (x = 0.09-0.91) alloy compounds is quite closed to the molar ratio of [Cl-BzPy][$Ni(mnt)_2$] to [Cl-BzPy][$Pt(mnt)_2$] in the starting materials. In addition to this, the Ni and Pt molar fractions were measured by energy dispersive

spectra (EDS) and inductively coupled plasma-mass spectra (ICP-MS), the results are shown in Table S2 and Table S3, which also in approximately agreement with the results obtained by the elemental analyses for C, H and N as well as the refinement of occupation factor of Ni/Pt in the crystal structures at 296 K.

The uniformity of the alloy sample is confirmed by DSC measurements (ref. next section), each sample showed one thermal anomaly peak (The sample should show several thermal anomaly peaks if it is a simple mixture comprised of several magnetic phase transition compounds with distinct T_C). The EDS mappings of Ni and Pt elements in **[Cl-BzPy][Ni$_x$Pt$_{1-x}$(mnt)$_2$]** (x = 0.09, 0.54 and 0.91) are given in Figure S2, which further demonstrated that the Ni and Pt elements uniformly distribute in the crystal of **[Cl-BzPy][Ni$_x$Pt$_{1-x}$(mnt)$_2$]**.

IR spectra of [Cl-BzPy][Ni$_x$Pt$_{1-x}$(mnt)$_2$] (x = 0.09-0.91) in 3190-550 cm^{-1} regime (Figure S3) are quite similar to each other besides two bands centered around 1160 and 890 cm^{-1}. The band around 1160 cm^{-1} is assigned to the $\nu_{C\text{-}S}$ + $\nu_{C\text{-}C}$, $\pi_{C\text{-}CN}$ vibrational models of mnt^{2-} ligand and the band around 890 cm^{-1} arises from the $\nu_{C\text{-}S}$ stretching vibration model of mnt^{2-} ligand.[18] Two characteristic bands in the IR spectrum of [Cl-BzPy][Pt(mnt)$_2$] locate in the higher wavenumber side compared with the IR spectrum of [Cl-BzPy][Ni(mnt)$_2$], and the maximums of two bands shift towards the higher wavenumber side with the Pt component increase in [Cl-BzPy][Ni$_x$Pt$_{1-x}$(mnt)$_2$] (ref. Figure 1).

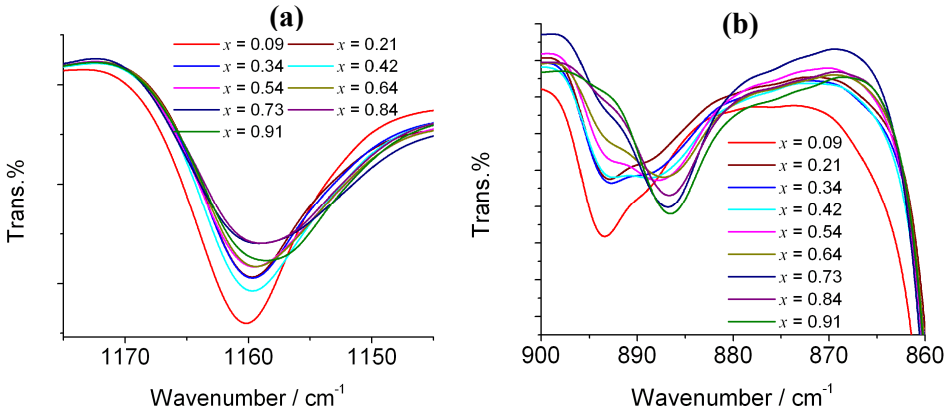

Figure 1 IR spectra of [Cl-BzPy][Ni$_x$Pt$_{1-x}$(mnt)$_2$] (x = 0.09-0.91) for the bands of the

$\nu_{C-S} + \nu_{C-C}$, π_{C-CN} and ν_{C-S} bands of mnt^{2-} ligands.

Crystal structures

Single crystal X-ray diffraction data for **[Cl-BzPy][Ni_xPt_{1-x}(mnt)$_2$]** (x = 0.09-0.91) were collected at 296 K for the high-temperature phase. Nine alloy compounds are isostructural to the parent compounds **[Cl-BzPy][Ni(mnt)$_2$]** and **[Cl-BzPy][Pt(mnt)$_2$]** with extremely analogous lattice parameters and the crystals belong to monoclinic space group *P2(1)/c* in high-temperature phase. As shown in Figure 2, the lengths of *a*- and *c*-axes are almost independent on the molar fraction x value, the *β* angle decrease gradually with x increase in high-temperature phase. It is noticeable that the *b*-axis length and cell volume show a reduce trend with x increase but the change is not monotonically.

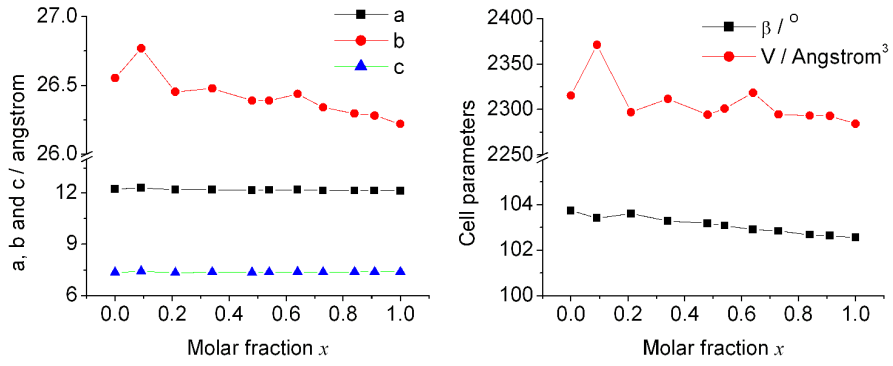

Figure 2 Cell parameters *a*, *b*, *c*, *β* and *V* as a function of the molar fraction *x* in the crystals of **[Cl-BzPy][Ni_xPt_{1-x}(mnt)$_2$]** (*x* = 0-1).

An asymmetric unit is comprised of one anion with one cation in high-temperature phase (ref. Figure 3a), indicating that the $[Ni(mnt)_2]^-$ and $[Pt(mnt)_2]^-$ anions are randomly distributed in the alloy crystal. The molecule and packing structures of **[Cl-BzPy][Ni_xPt_{1-x}(mnt)$_2$]** (x = 0.09-0.91) are rather similar to the parent compounds **[Cl-BzPy][Ni(mnt)$_2$]** and **[Cl-BzPy][Pt(mnt)$_2$]**. The bond lengths and bond angles in anion moiety are summarized in Table 3, and the averaged d_{M-S} and ∠S-M-S bite angle in an anion moiety are presented in Figure 3b for **[Cl-BzPy][Ni_xPt_{1-x}(mnt)$_2$]** (x = 0.09–0.91) together with two parent compounds, which show the d_{M-S} value reduces gradually while the ∠S-M-S value raises a little

with x increase.

The segregated and uniform stacks of both anions and cations are formed in the alloy crystals **[Cl-BzPy][Ni_xPt_{1-x}(mnt)$_2$]** (x = 0.09-0.91), such a packing structure is analogous to the parent compounds **[Cl-BzPy][Ni(mnt)$_2$]** and **[Cl-BzPy][Pt(mnt)$_2$]**. As displayed in Figure 3c and 3d, the anion and cation stacks run along *c*-axis direction, with two anions and two cations per unit. Each anion stack is surrounded by four cation stacks and vice versa. The neighboring anions show a little slippage along the longer molecule axis with a small rotation within an anion stack and the adjacent cations are aligned in a boat-conformation manner within a cation stack. The typical intermolecular separations within an anion or a cation stack as well as between the neighboring anion and cation stacks are summarized in Table S1 and given in ESI.

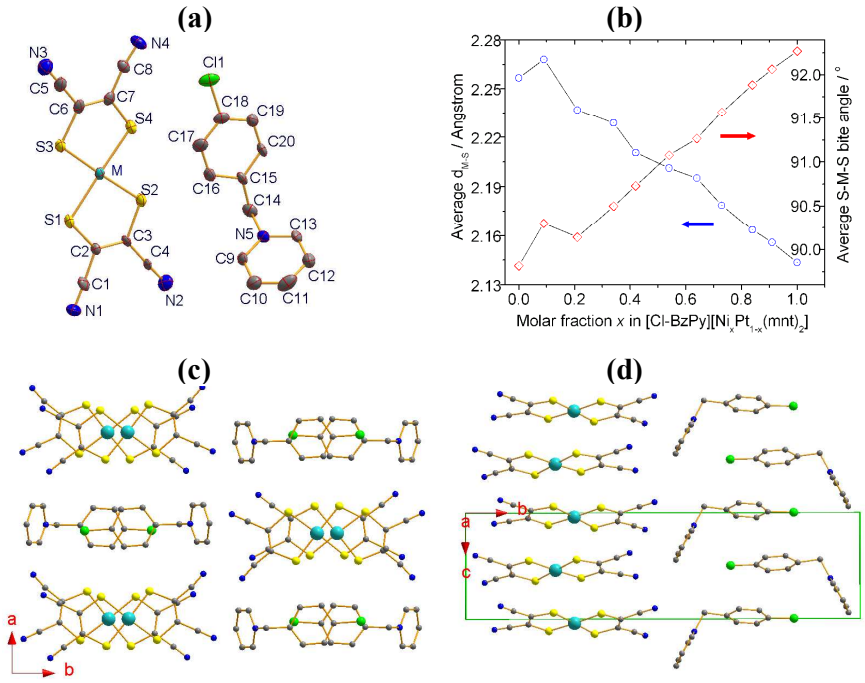

Figure 3 (a) An asymmetric unit with non-hydrogen atom labeling (b) average M-S bond length and ∠S-M-S bite angle in $[M(mnt)_2]^-$ (M = Ni or Pt) moiety (c, d) packing diagrams viewed along c- and a-axes directions, respectively, in **[Cl-BzPy][Ni_xPt_{1-x}(mnt)$_2$]** (*x* = 0-1).

The single crystal X-ray diffraction data of **[Cl-BzPy][Ni_xPt_{1-x}(mnt)$_2$]** (*x* =

0.09, 0.54 and 0.91) in LT-phase were collected at 100 K, and the details about data collection, structure refinement and crystallography are summarized in Table S4. Since there are diffuse diffractions in the wide temperature range around the magnetic transition, which arise from the strongly magnetoelastic interaction in the 1-D antiferromagnetic chain system and affect the precision of the intensity of Bragg diffraction,[11] the R(sigma) values of diffraction data for these spin-Peierls-like compounds become large, leading to R_1 and wR_2 values being higher as well as the precision of some bonds being lower in low-temperature phase.

From the high-temperature to low-temperature phase, the space group of **[Cl-BzPy][Ni_xPt_{1-x}(mnt)$_2$]** (x = 0.09, 0.54 and 0.91) degrades from *P2(1)/c*, with point group C_{2h} and four symmetry elements (E, C_2, i and σ_h), to *P-1*, with point group C_i and two symmetry elements (E and i), while the Z values remain the same (Z = 4), this suggests that symmetry breaking undergoes across this phase transition from a macroscopic viewpoint. The 2-fold screw axis and the glide plane along the *c*-axis disappeared from the high-temperature to low-temperature phase make that the symmetry related species (anions and cations) through the 2-fold screw axis and the glide plane are inequivalent in a unit cell, as a result, an asymmetric unit switches from a pair of anion-cation in high-temperature phase into two pairs of anions and cations in low-temperature phase (as shown in Figure S6). It is noticeable that the $[Ni(mnt)_2]^-$ and $[Pt(mnt)_2]^-$ anions still show random distribution at 100 K. In our earlier study, it was found that the $[Ni(mnt)_2]^-$ and $[Au(mnt)_2]^-$ anions in an alloy family of **[NO_2-BzPy][Ni_xAu_{1-x}(mnt)$_2$]** (where NO_2-BzPy$^+$ = 4'-nitrobenzyl-1-pyridinium) showed random distribution within a stack when temperature is down to 10 K.[11] The packing structure changes mostly concern that the regular stacks of both anion and cation in high-temperature phase dimerize in low-temperature phase for **[Cl-BzPy][Ni_xPt_{1-x}(mnt)$_2$]** (x = 0.09, 0.54 and 0.91).

Magnetic, thermal and spin-Peierls-type transition features

Plots of molar magnetic susceptibility (χ_m) *vs* temperature are displayed in

Figure 4 for **[Cl-BzPy][Ni_xPt_{1-x}(mnt)$_2$]** (x = 0.09-0.91). The alloy compounds show similar magnetic behaviors in 2-300 K range besides the different T_C, namely, the magnetic nature of 1-D Heisenberg antiferromagnetic chain-like in high-temperature phase and the feature of spin-gap-like below magnetic transition as well as a Curie-Weiss type magnetic behaviour in low-temperature region which is caused by the lattice defects. It is analogous to the parent compounds that the magnetic phase transition is associated with the symmetry-broking structural phase transition, this was confirmed by the crystal structural analysis in low-temperature phase for the alloy compounds **[Cl-BzPy][Ni_xPt_{1-x}(mnt)$_2$]** (x = 0.09, 0.54 and 0.91). The $[Ni(mnt)_2]^-$ and $[Pt(mnt)_2]^-$ anions randomly distribute within a stack in both high- and low-temperature phases, resulting in the alloy compounds becoming random spin systems. As a result, it is hard to fit the magnetic susceptibility data in both high- and low-temperature phases owing to the absence of suitable expression of magnetic susceptibility versus temperature for a random spin system, and it is unavailable to get the parameters of J in high-temperature phase and Δ in low-temperature phase.

The critical temperature of magnetic transition, defined by the knee-point temperature in the plot of χ_m-T, decreases with x increase for **[Cl-BzPy][Ni_xPt_{1-x}(mnt)$_2$]** (x = 0.09-0.91). Differential scan calorimetric (DSC) measurements were further performed in the temperature range of 98-293 K for precisely determining the transition temperature T_C of these alloys. The curves of heat flow versus temperature are shown in Figure 5a, where the thermal anomaly peak shifts to lower temperature side with x increase, and the plot of T_{peak} *vs* molar fraction x is displayed in Figure 5b for [Cl-BzPy][Ni_xPt_{1-x}(mnt)$_2$] (x = 0.09-0.91), it is worthy of noting that the T_{peak} (or T_C) is linearly correlated with the molar fraction x, which can be expressed using the Eq. (1). We get T_C = 280 and 107 K using Eq. (1) when x = 0 and 1, respectively, which is close to T_C of two parent compounds.

$$T_{peak}(\text{or } T_C) = 280(3)-173(5)x \qquad (1)$$

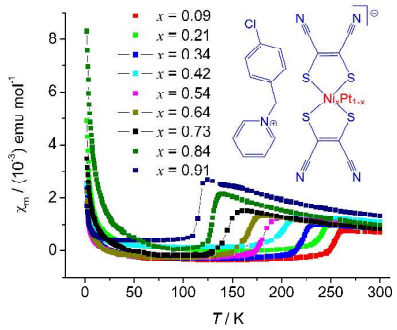

Figure 4 Plots of χ_m-T for **[Cl-BzPy][Ni$_x$Pt$_{1-x}$(mnt)$_2$]** (x = 0.09-0.91) in the temperature range 2-300 K.

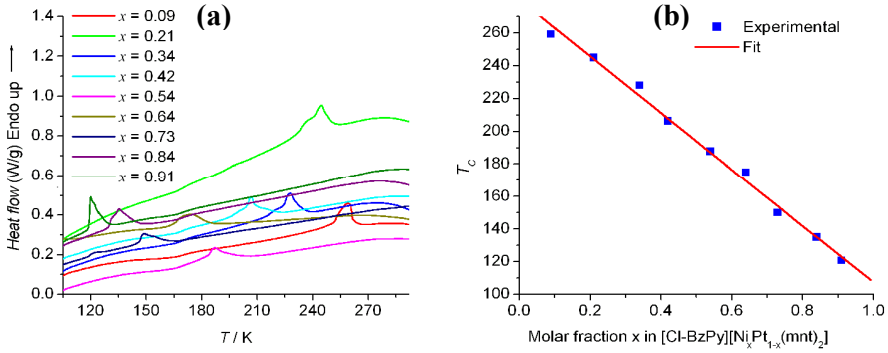

Figure 5 (a) DSC plots of **[ClBzPy][Ni$_x$Pt$_{1-x}$(mnt)$_2$]** (x = 0.09-0.91) in the temperature range 93-293 K (b) T_C-x plot.

Conclusion

In summary, we achieved a molecular alloy family with a formula **[ClBzPy][Ni$_x$Pt$_{1-x}$(mnt)$_2$]** (x = 0.09-0.91). $[Ni(mnt)_2]^-$ and $[Pt(mnt)_2]^-$ anions show homogeneous in distribution and this family shows a good linear relationship between the magnetic transition temperature, T_C, and the molar fraction x of the component, indicating that the magnetic transition temperature can be precisely controlled and consecutively tuned in this alloy family.

Supporting data

CCDC 892052-892060 contain the supplementary crystallographic data for compounds [ClBzPy][Ni$_x$Pt$_{1-x}$(mnt)$_2$] (x = 0.09-0.91). These data can be obtained free of charge via http://www.ccdc.cam.ac.uk/conts/retrieving.html, or from the

Cambridge Crystallographic Data Centre, 12 Union Road, Cambridge CB2 1EZ, UK; fax: (+44) 1223-336-033; or e-mail: deposit@ccdc.cam.ac.uk.

Acknowledgment

Authors thank the Priority Academic Program Development of Jiangsu Higher Education Institutions and National Nature Science Foundation of China for financial support (grant no. 91122011 and 21271103).

References and Notes

1. R. E. Peierls, *Quantum Theory of Solids*, Oxford University Press, London, England, 1955, p. 108.
2. J. W. Bray, H. R. Hart, L. V. Interrante Jr., L. S. Jacobs, J. S. Kasper, G. D. Watkins, S. H. Wee, *Phys. Rev. Lett.* 1975, **35**, 744.
3. R. K. Kremer, I. Loa, F. S. Razavi, K. Syassen, *Solid State Commun.* 2000, **113**, 217.
4. S. Huizinga, J. Kommandeur, G. A. Sawatzky, B. T. Thole, K. Kopinga, W. J. M. de Jonge, J. Roos, *Phys. Rev. B* 1979, **19**, 4723.
5. M. Hase, I. Terasaki, K. Uchinokura, *Phys. Rev. Lett.* 1993, **70**. 3651.
6. Y. Nakazawa, A. Sato, M. Seki, K. Saito, K.-i. Hiraki, T. Takahashi, K. Kanoda, M. Sorai, *Phys. Rev. B* 2003, **68**, 085112.
7. X. M. Ren, T. Akutagawa, S. Nishihara, T. Nakamura, W. Fujita, K. Awaga, *J. Phys. Chem. B* 2005, **109**, 16610.
8. M. Shaz, S. van Smaalen, L. Palatinus, M. Hoinkis, M. Klemm, S. Horn, R. Claessen, *Phys. Rev. B* 2005, **71**, 100405(R).
9. R. D. Willett, C. J. G. Garcrá, B. L. Ramakrishna, B. Twamley, *Polyhedron* 2005, **24**, 2232.
10. Y. J. Wang, Y. J. Kim, R. J. Christianson, S. C. LaMarra, F. C. Chou, R. J. Birgeneau, *J. Phys. Soc. Jap.* 2003, **72**, 1544.
11. X. M. Ren, T. Akutagawa, S. Noro, S. Nishihara, T. Nakamura, Y. Yoshida, K. Inoue, *J. Phys. Chem. B* 2006, **110**, 7671.
12. S. B. Oseroff, S. W. Cheong, B. Aktas, M. F. Hundley, Z. Fisk, L. W. Rupp Jr., *Phys. Rev. Lett.* 1995, **74**, 1450.
13. C. Stock, S. Wakimoto, R.J. Birgeneau, S. Danilkin, J. Klenke, P. Smeibidl, P. Vorderwisch, *J. Phys. Soc. Jap.* 2005, **74**, 746.
14. X. M. Ren, Q. J. Meng, Y. Song, C. S. Lu, C. J. Hu, X. Y. Chen, *Inorg. Chem.* 2002, **41**, 5686.
15. X. M. Ren, H. Okudera, R. K. Kremer, Y. Song, C. He, Q. J. Meng, P. H. Wu,

Inorg. Chem. 2004, **43**, 2569.

16. *Software packages SMART and SAINT*, Siemens Analytical X-ray Instrument Inc., Madison, WI, 1996.
17. G. M. Sheldrick, *SHELX-97, Program for the refinement of crystal structure*, University of Göttingen, Germany, 1997.
18. C. W. Schläpfer, K. Nakamoto, *Inorg. Chem.* 1975, **14**, 1338.

Table 1 Crystallographic data for compounds [Cl-BzPy][$Ni_xPt_{1-x}(mnt)_2$] (x = 0-1) at ambient temperature

Compound	x = 0[15]	x = 0.09	x = 0.21	x = 0.34	x = 0.42	x = 0.54
Temp. / K	293(2) K	296(2) K	296(2) K	296(2) K	296(2) K	296(2) K
λ / Å	0.71073					
FW	680.12	668.06	651.53	634.28	622.36	607.76
Crystal system	Monoclinic					
SG	P2(1)/c					
CCDC no.	187749	892052	892053	892054	892055	892056
a / Å	12.220(3)	12.291(9)	12.173(5)	12.187(2)	12.1496(19)	12.1562(16)
b / Å	26.555(6)	26.77(2)	26.453(11)	26.477(5)	26.389(4)	26.389(3)
c / Å	7.3450(17)	7.409(6)	7.339(3)	7.3604(13)	7.3488(12)	7.3638(10)
β / °	103.734(4)	103.408(6)	103.596(5)	103.279(2)	103.166(2)	103.069(2)
V / $Å^3$ / Z	2315.3(9)/4	2371(3)/4	2297.0(16)/4	2311.5(7)/4	2294.2(6)/4	2301.0(5)/4
ρ / $g·cm^{-1}$	1.951	1.871	1.884	1.823	1.802	1.754
F(000)	1300	1282	1258	1233	1215	1194
Abs.coeff. / mm^{-1}	6.555	5.949	5.503	4.807	4.383	3.807
Data coll. θ range /°	2.30-25.00	2.28-27.30	2.31- 26.92	2.31-26.16	2.31-26.00	2.31-26.00
Index range	-13≤h≤14	-15≤h≤12	-15≤h≤13	-15≤h≤12	-14≤h≤14	-14≤h≤14
	-31≤k≤29	-34≤k≤28	-33≤k≤33	-32≤k≤32	-30≤k≤32	-32≤k≤26
	-8≤l≤8	-9≤l≤9	-9≤l≤8	-9≤l≤9	-9≤l≤9	-9≤l≤9
R_{int}	0.1490	0.1588	0.1374	0.2519	0.0584	0.0560
Reflect. /restraints/parameters	4053/0/280	5227/0/281	4847/0/282	4563/0/282	4497/0/281	4506/2/281
Refinement method	Full-matrix least-squares on F^2					
Goodness of fit on F^2	0.999	1.106	0.975	0.997	1.039	1.048
R1, wR2 [I>2σ(I)]	0.0593, 0.1172	0.1380, 0.3339	0.0790, 0.1821	0.0837, 0.2166	0.0413, 0.0910	0.0422, 0.1048
R1, wR2 [all data]	0.0886, 0.1242	0.2105, 0.3735	0.1340, 0.2152	0.1042, 0.2338	0.0604, 0.0972	0.0561, 0.1099
Residual /e·$Å^{-3}$	3.469/-1.401	3.945/-5.995	4.164/-3.511	3.893/-1.605	0.960/-0.685	1.056/-0.643

$R_1 = \sum||F_o| - |F_c||/|F_o|$, $wR_2 = [\sum w(\sum F_o^2 - F_c^2)^2/\sum w(F_o^2)^2]^{1/2}$

Table 1 (continued).

Compound	x = 0.64	x = 0.73	x = 0.84	x = 0.91	x = 1[14]
Temp. / K	296(2) K	296(2) K	296(2) K	296(2) K	296(2) K
λ / Å			0.71073		
FW	593.51	581.10	564.93	555.35	543.74
Crystal system			Monoclinic		
SG			P2(1)/c		
CCDC no.	892057	892058	892059	892060	158525
a / Å	12.177(3)	12.1309(16)	12.121(2)	12.1224(15)	12.105(2)
b / Å	26.438(7)	26.340(4)	26.296(4)	26.281(3)	26.218(4)
c / Å	7.3875(19)	7.3653(10)	7.3747(13)	7.3751(9)	7.374(2)
β / °	102.900(3)	102.839(2)	102.672(2)	102.627(2)	102.55(2)
V / Å^3 / Z	2318.3(10)/4	2294.5(5)/4	2293.3(7)/4	2292.8(5)/4	2284.2(9)/4
ρ / g·cm^{-1}	1.700	1.682	1.636	1.609	1.581
F(000)	1173	1155	1131	1117	1100
Abs. coeff. / mm^{-1}	3.234	2.788	2.164	1.794	1.350
Data collect. θ Range / °	2.31- 27.71	2.31-26.37	2.32- 27.47	2.32- 27.61	1.89-25.00
Index range	-15≤h≤15 -34≤k≤34 -9≤l≤9	-15≤h≤15 -32≤k≤32 -9≤l≤9	-15≤h≤15 -33≤k≤33 -9≤l≤9	-15≤h≤15 -34≤k≤33 -9≤l≤9	-14≤h≤14 -31≤k≤1 -1≤l≤8
R_{int}	0.0790	0.0537	0.0566	0.0516	0.0455
Reflect. /restraints/parameters	5384 / 0 / 281	4672 / 2 / 282	5235 / 4 / 282	5294 / 0 / 282	3997 / 0 / 294
Refinement method			Full-matrix least-squares on F^2		
Goodness of fit on F^2	1.044	1.029	1.030	1.019	1.023
R1, wR2 [I>2σ(I)]	0.0592, 0.1418	0.0415, 0.1041	0.0448, 0.0991	0.0408, 0.0891	0.0460, 0.1065
R1, wR2 [all data]	0.1027, 0.1611	0.0579, 0.1130	0.0721, 0.1120	0.0698, 0.1011	0.0773, 0.1226
Residual /e·Å^{-3}	1.025/ -0.871	0.775/-0.485	0.755/ -0.546	0.409/ -0.332	0.457/ -0.426

$R_1 = \sum||F_o| - |F_c||/|F_o|$, $wR_2 = [\sum w(\sum F_o^2 - F_c^2)^2/\sum w(F_o^2)^2]^{1/2}$

Table 2: Elemental analyses (C, H, N), the molar ratio of **[Cl-BzPy][Ni(mnt)$_2$]** to **[Cl-BzPy][Pt(mnt)$_2$]** from the starting materials and the occupation factor of Ni to Pt in the crystal structural refinement for **[Cl-BzPy][Ni$_x$Pt$_{1-x}$(mnt)$_2$]** (x = 0.09-0.91).

Alloy	Calculated			Found			Ni:Pt[a]	Ni:Pt[b]
	C	H	N	C	H	N		
x = 0.09	37.98	1.75	11.07	37.95	1.76	11.03	0.1:0.9	0.09:0.91
x = 0.21	38.99	1.80	11.37	38.98	1.79	11.40	0.2:0.8	0.21:0.79
x = 0.34	40.15	1.85	11.71	40.12	1.85	11.73	0.3:0.7	0.34:0.66
x = 0.42	40.89	1.89	11.92	40.87	1.88	11.89	0.4:0.6	0.42:0.58
x = 0.54	42.07	1.94	12.26	42.09	1.93	12.23	0.5:0.5	0.54:0.46
x = 0.64	43.10	1.99	12.56	43.11	1.98	12.53	0.6:0.4	0.64:0.36
x = 0.73	44.07	2.03	12.85	44.06	2.01	12.89	0.7:0.3	0.73:0.27
x = 0.84	45.31	2.09	13.21	45.25	2.11	13.19	0.8:0.2	0.84:0.16
x = 0.91	46.14	2.13	13.45	46.16	2.12	13.51	0.9:0.1	0.91:0.09

[a] Molar ratio in the starting material; [b] Occupation factor ratio obtained from the crystal structural refinement.

Table 3: Coordinated Bond Lengths (Å) and Angles (deg) in an anionic moiety for **[Cl-BzPy][$Ni_xPt_{1-x}(mnt)_2$]** (x = 0-1)

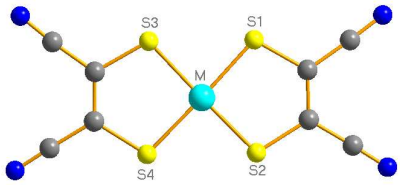

x	M-S1	M-S2	M-S3	M-S4	S1-M-S2	S3-M-S4
0[a]	2.2550(25)	2.2611(26)	2.2469(25)	2.2636(26)	89.779(96)	89.848(97)
0.09[b]	2.2690(31)	2.2582(39)	2.2923(37)	2.2522(38)	90.416(126)	90.187(1330
0.21[b]	2.2470(13)	2.2285(14)	2.2416(14)	2.2303(15)	90.024(50)	90.251(49)
0.34[b]	2.2456(27)	2.2132(26)	2.2255(29)	2.2299(25)	90.64(11)	90.36(11)
0.42[b]	2.2238(13)	2.2036(13)	2.1997(13)	2.2152(13)	90.716(51)	90.742(51)
0.54[b]	2.2165(13)	2.1945(13)	2.1903(13)	2.2042(13)	91.060(49)	91.092(51)
0.64[b]	2.1843(17)	2.1972(17)	2.2115(17)	2.1881(17)	91.306(63)	91.214(62)
0.73[b]	2.1671(11)	2.1801(10)	2.1955(11)	2.1721(10)	91.559(40)	91.577(40)
0.84[b]	2.1542(9)	2.1647(9)	2.1776(9)	2.1570(9)	91.850(34)	91.916(33)
0.91[b]	2.1477(8)	2.1557(8)	2.1694(8)	2.1502(8)	92.048(31)	92.084(31)
1[b]	2.1447(11)	2.1391(12)	2.1395(12)	2.1509(12)	92.173(45)	92.372(46)

[a]Temperature = 293 K; [b]Temperature = 296 K

Table of Contents

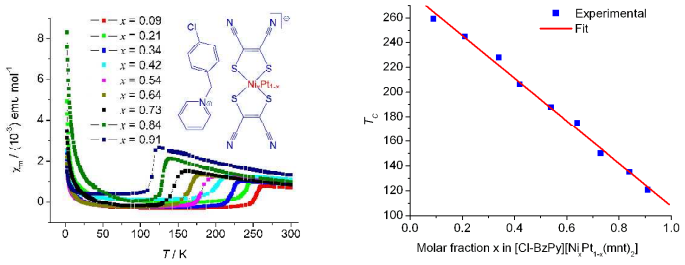

The magnetic transition system with precisely tunable T_C was achieved through formation of molecule alloy and T_C is linearly correlated with the molar fraction x.